Supplement of

Simulating the radiative forcing of oceanic dimethylsulfide (DMS) in Asia based on Machine learning estimates

Junri Zhao et al.

Correspondence to: Yan Zhang (yan_zhang@fudan.edu.cn)

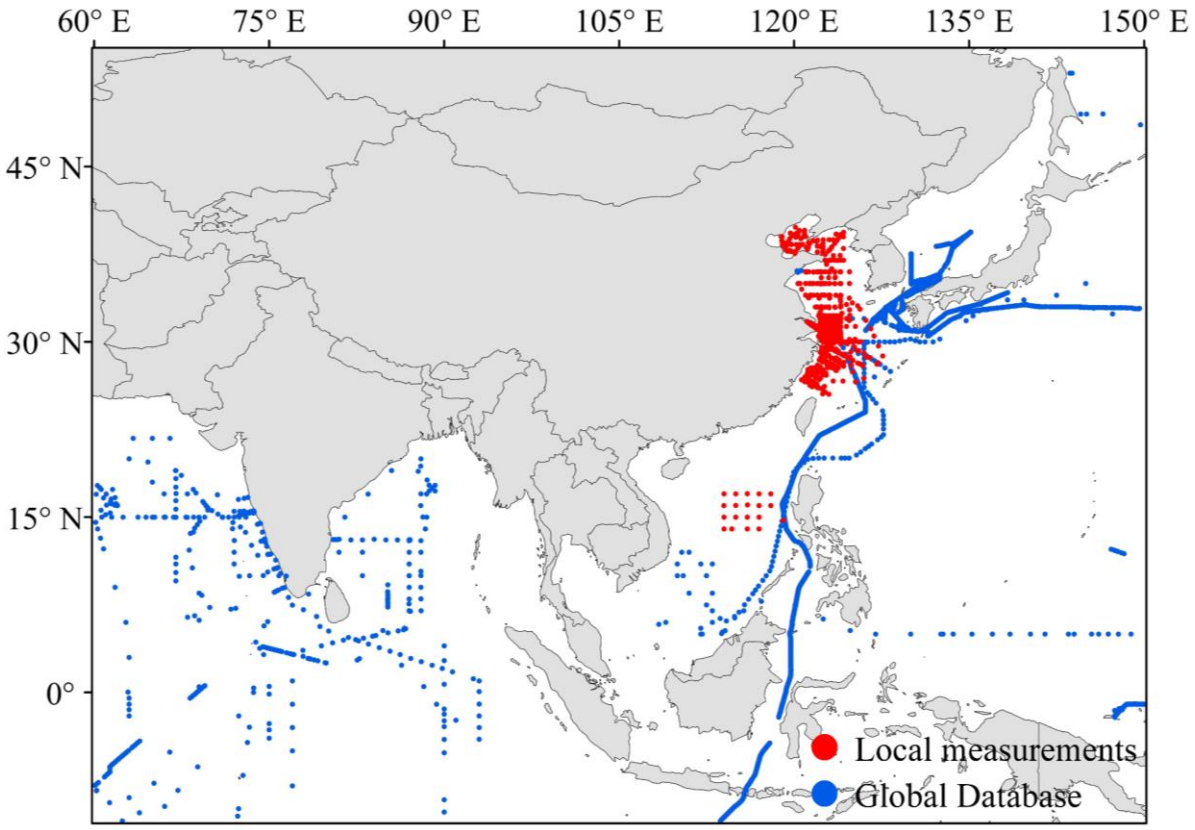

Figure S1. Spatial distribution of DMS measurements in simulation domain (11°S to 55°N, 60–150°E).

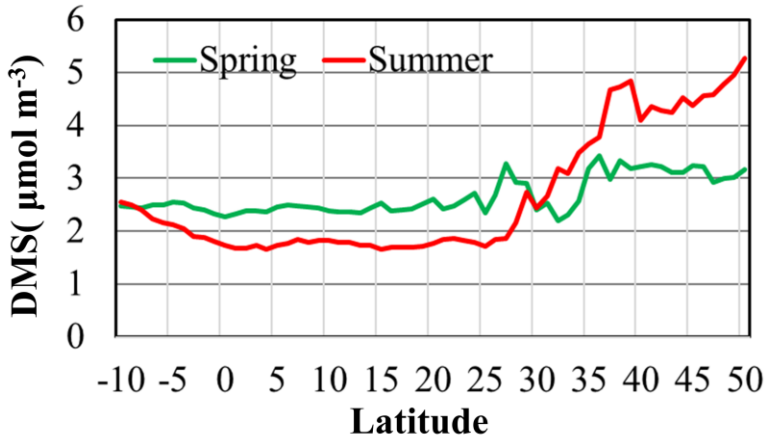

Figure S2. Zonal mean DMS sea-surface concentrations predicted by XGBoost between -10 to 50° latitude band of entire simulation domain (11°S to 55°N, 60–150°E).

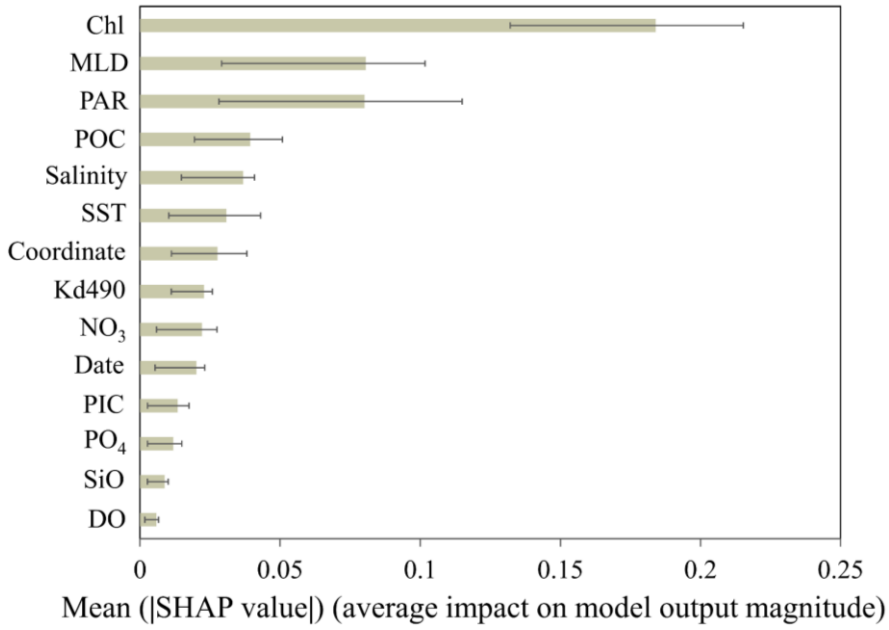

Figure S3. The ranked mean SHAP values of each predictor across all prediction cases, and the line ranges represent the upper and lower quantile (25th–75th percentile) across the distribution.

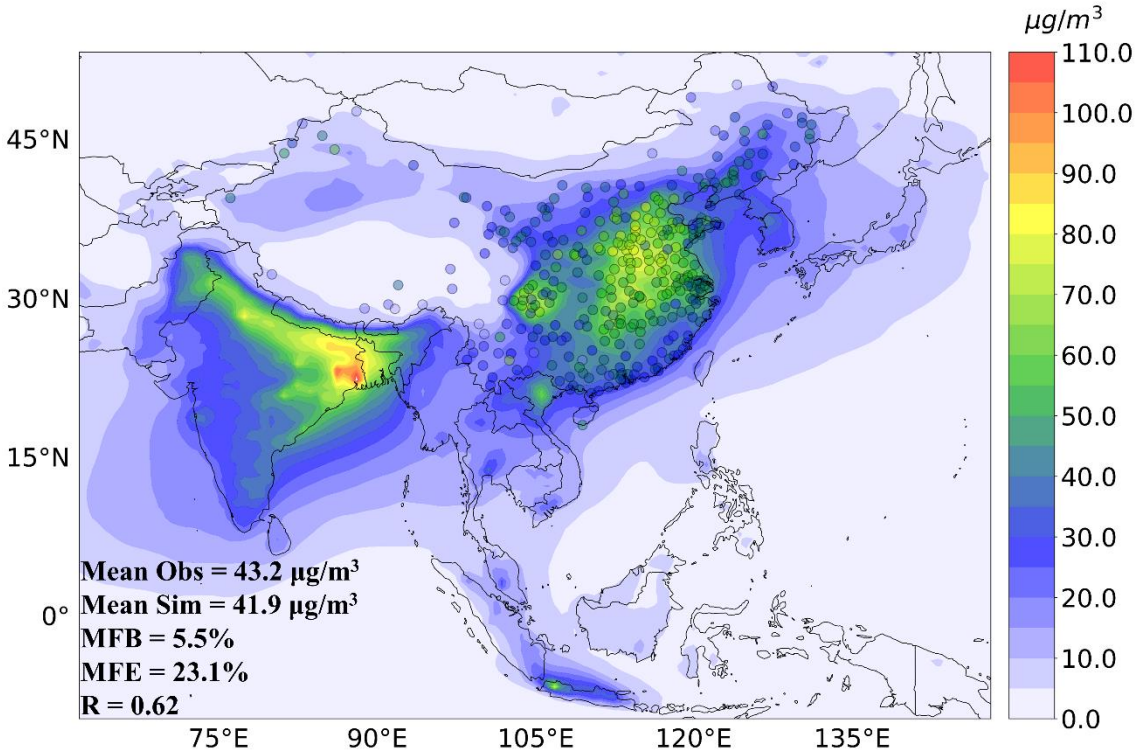

Figure S4. Spatial plots of annual mean concentrations from XG simulation (background plots) and observed (circles) values of $PM_{2.5}$. The mean observation (Mean Obs), mean simulation (Mean Sim), mean fractional error (MFE), and mean fractional bias (MFB) displayed at lower left corner are the statistic result of averaged 365 grids.

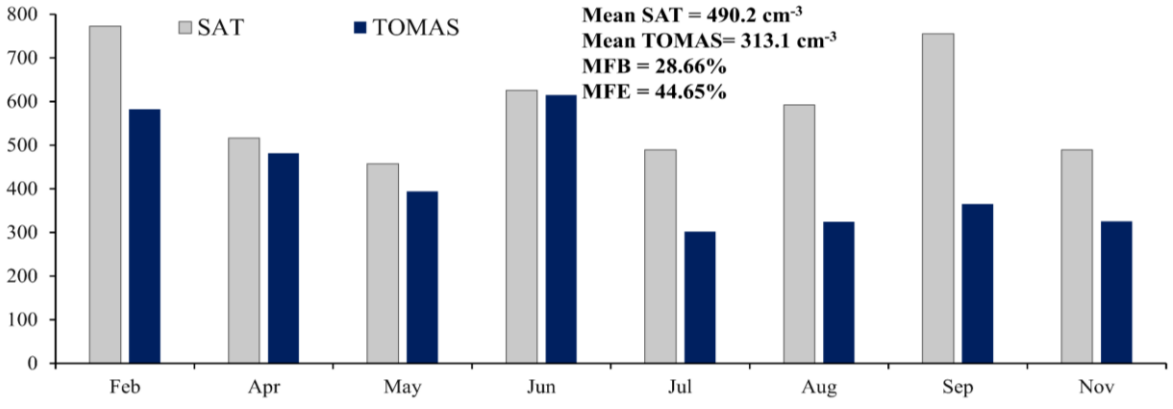

Figure S5. Monthly mean simulated CCN concentrations (TOMAS) from XG simulation and satellite-retrieved CCN concentrations (SAT) from Liu et al., (2020). The mean satellite-retrieved (Mean SAT) CCN concentrations, mean simulation (Mean TOMAS), mean fractional error (MFE), and mean fractional bias (MFB) displayed at upper centre are the statistic result of averaged on the simulation grid for corresponding satellite-retrieved CCN geographical location (in total 667 grids).

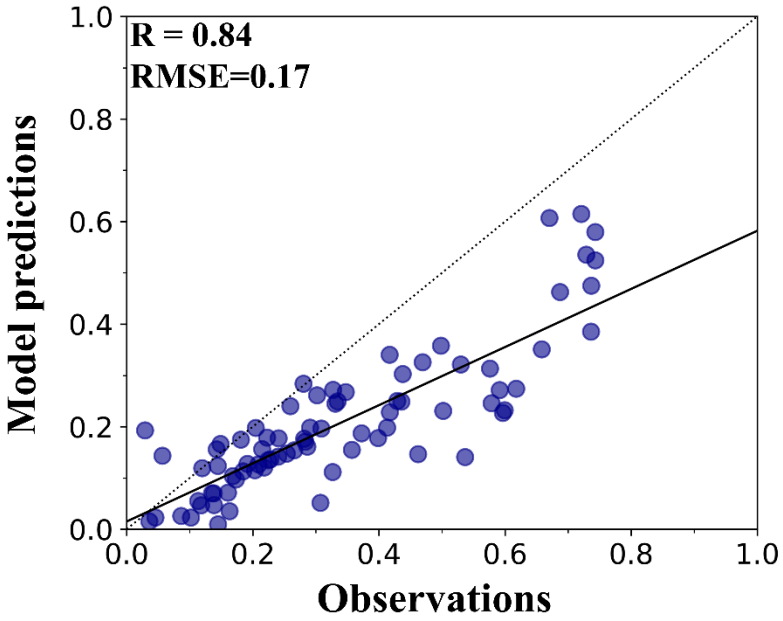

Figure S6. The scatter plot of AOD compares annual mean model predictions (XG simulation) and observations from AERONET. The black solid line and dashed line indicate trendline and 1:1 line, respectively.

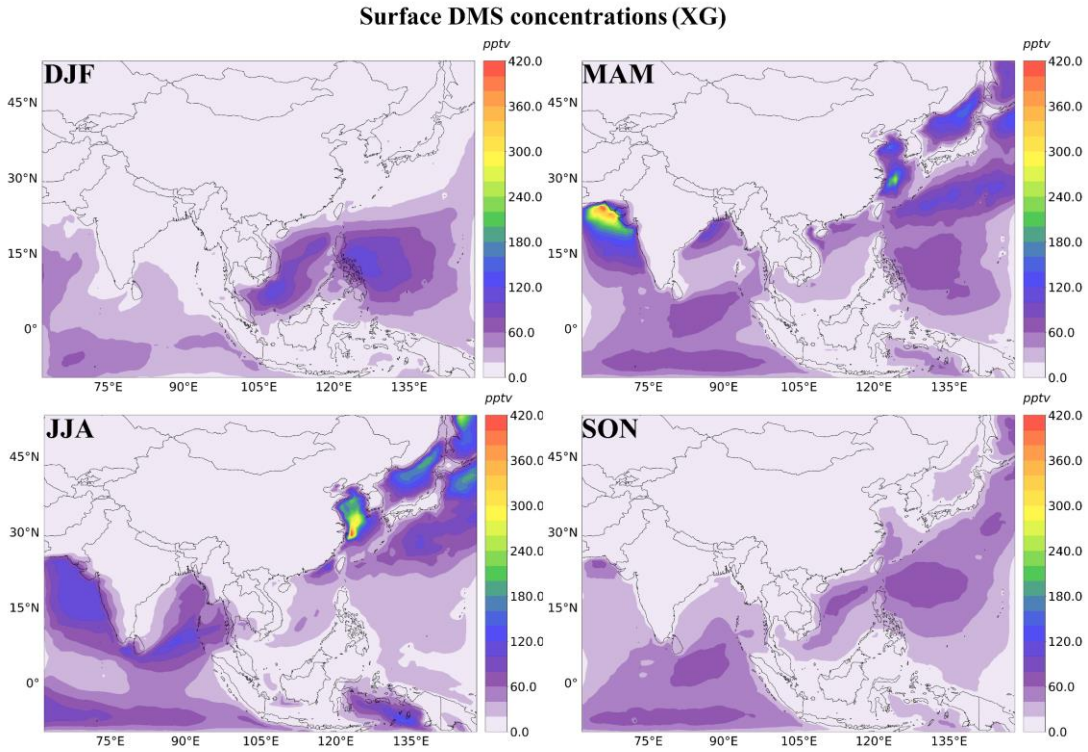

Figure S7. Seasonal variations of atmospheric surface DMS concentrations estimated by the XG simulation.

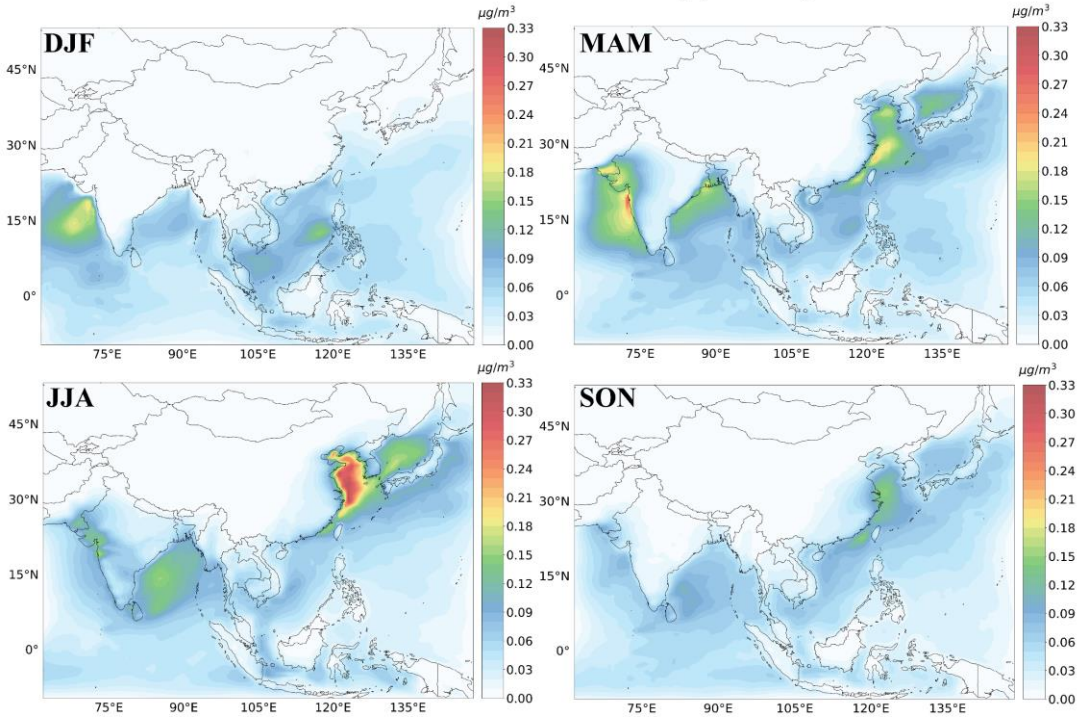

40

41 **Figure S8.** Seasonal variations of absolute changes in surface SO_2 between the XG and ND (no DMS) simulations.

42

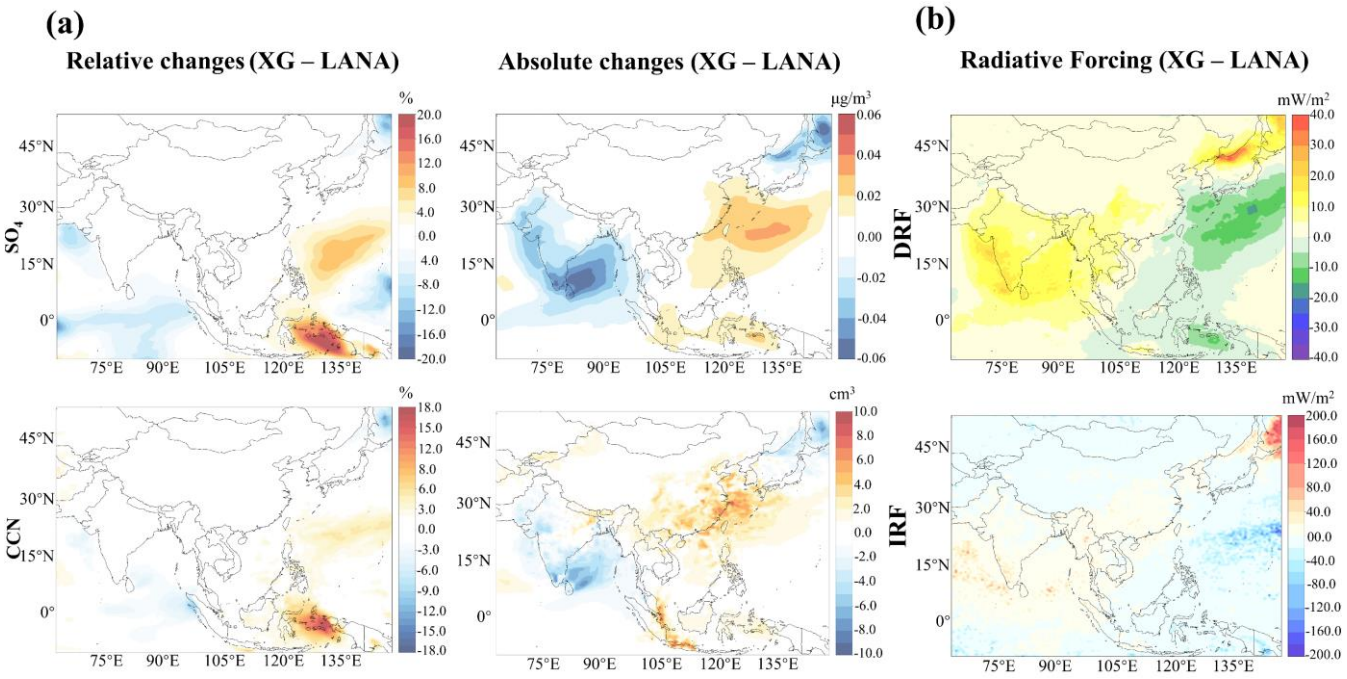

43

Figure S9. Panel (a) presents the spatial distributions of annual mean percent changes and absolute changes in surface SO_4^{2-} and CCN, and panel (b) presents the spatial distributions of annual mean all-sky DRF and cloud-albedo IRF between the XG and LANA simulations.

Table S1. Training dataset participated in machine learning estimates.

Variables	units	Filtering threshold	sources
DMS measurements in China Seas	μmol m^{-3}	Remove values < 0.1 and values >100	Local measurements from Ocean University of China (Yang et al., 2015a;Yang et al., 2014;Yang et al., 2015b;Li et al., 2020b;Li et al., 2020a)
DMS measurements from global database	μmol m^{-3}	Remove values < 0.1 and values >100	http://saga.pmel.noaa.gov/dms/ (Kettle et al., 1999;Lana et al., 2011)
Salinity	unitless	Remove values < 30 and sampling depth >10m	https://www.ncei.noaa.gov/products/world-ocean-atlas (Garcia et al., 2019)
Sea surface temperature (SST)	°C	-	https://www.ncei.noaa.gov/products/world-ocean-atlas (Garcia et al., 2019)
Dissolved Oxgyen (DO)	μmol kg^{-1}	Remove values < 0.01	https://www.ncei.noaa.gov/products/world-ocean-atlas (Garcia et al., 2019)
Silicate	μmol kg^{-1}	Remove values < 0.01	https://www.ncei.noaa.gov/products/world-ocean-atlas (Garcia et al., 2019)
Phosphate	μmol kg^{-1}	Remove values < 0.01	https://www.ncei.noaa.gov/products/world-ocean-atlas (Garcia et al., 2019)
Nitrate	μmol kg^{-1}	Remove values < 0.01	https://www.ncei.noaa.gov/products/world-ocean-atlas (Garcia et al., 2019)
Mixed layer depth (MLD)	m	Remove values >150	https://www.pmel.noaa.gov/mimoc/ (Schmidtko et al., 2013)
Chlorophyll concentration (Chl)	mg m^{-3}	Remove values < 0.01	https://oceancolor.gsfc.nasa.gov/l3
Diffuse attenuation coefficient at 490m (kd490)	m^{-1}	-	https://oceancolor.gsfc.nasa.gov/l3
Particulate Inorganic Carbon (PIC)	mg m^{-3}	-	https://oceancolor.gsfc.nasa.gov/l3
Particulate organic Carbon (POC)	mg m^{-3}	-	https://oceancolor.gsfc.nasa.gov/l3
Photosynthetically available Radiation (PAR)	Einstein m^{-2} d^{-1}	-	https://oceancolor.gsfc.nasa.gov/atbd/par/

Table S2. Model performance for sea surface DMS concentration predictions.

	OBS	PRE	MB	RMSE	NMB
Winter	1.99	1.65	-0.34	1.69	-16.87

Spring	2.92	2.71	-0.21	1.81	-6.51
Summer	3.93	3.58	-0.35	2.19	-11.82
Fall	2.87	2.28	-0.59	2.08	-19.36
Annual average	2.57	2.31	-0.26	1.97	-10.28

Notes: OBS: mean observation value; PRE: mean prediction value; MB: mean bias; RMSE: root mean squared error; NMB: normalized mean bias.

Table S3. Comparison of seasonal mean DMS concentrations over Asia region from other studies (μmol m^{-3}).

Season	This study	Lana et al. (2011)	Wang et al. (2020)
Winter	1.93	1.78	1.30
Spring	2.52	2.33	2.21
Summer	2.19	2.01	1.81
Fall	2.03	1.87	1.71

Table S4. Comparison of regional mean modelled atmospheric DMS concentrations with observations from Cruise Survey Experiment (CSE) 1-3(Units: pptv).

	CSE 1	CSE 2	CSE 3
OBS	39.74	57.82	217.51
XG	46.42	41.65	334.90
LANA	23.40	36.71	95.94
OBS-XG	6.68	-16.17	117.39
OBS-LANA	-16.34	-21.11	-121.57

Notes: OBS refer to observations; XG and LANA refer to simulation values; OBS-XG and OBS-LANA refer to differences between observations and simulation values (XG and LANA).

Table S5. Comparison of mean annual CCN predictions from other studies (Units: cm^{-3})

City	Longitude	Latitude	CCN_obs	CCN_sim	Sources
Nanjing	118.7°E	32.06°N	1540.5	919.1	(Liu et al., 2020)
Nanjing	118.7°E	32.21°N	1669.2	994.3	(Liu et al., 2020)

Shanghai	121.29°E	31.18°N	2783.0	983.3	(Liu et al., 2020)
Guangzhou	113.21°E	23.07°N	1299.3	796.9	(Liu et al., 2020)
Shenzhen	114.56°E	22.48°N	1289.0	501.9	(Liu et al., 2020)
Taiwan	121.54°E	25.3°N	1010.5	325.4	(Cheung et al., 2020)
Indo-Gangetic Plain	85.81°E	20.24°N	2250.0	948.7	(Jayachandran et al., 2020)
Indo-Gangetic Plain	82.85°E	25.45°N	1650.0	1432.4	(Jayachandran et al., 2020)
Indo-Gangetic Plain	73.04°E	26.25°N	1375.0	602.2	(Jayachandran et al., 2020)
Eastern Himalaya	88.2°E	27°N	1800.0	1787.7	(Roy et al., 2017)
Central Himalaya	79.5°E	29.4°N	1000.0	1232.0	(Dumka et al., 2015)
Hyderabad	78.38°E	17.45°N	1100.0	1564.2	(Varghese et al., 2016)
Mahabaleshwar	73.4°E	17.6°N	1500.0	670.0	(Leena et al., 2016)

Table S6. Comparison of modelled annual mean DRF and IRF for DMS induced sulfate reported in previous studies.

Annual Mean DRF (W m^{-2})	Annual Mean IRF (W m^{-2})	Model	Sources
-0.23	-0.76	GLOMAP-mode global aerosol microphysics model	(Rap et al., 2013)
-0.074	-0.23	CESM-CAM5	(Yang et al., 2017)
--	-6.55	CESM-CAM5	(Jin et al., 2018)
--	-2.0	ECHAM5-HAMMOZ	(Thomas et al., 2010)
--	-1.79	ECHAM5-HAMMOZ	(Mahajan et al., 2015)

Notes: -- represents corresponding values that have not reported in their studies.

References:

Cheung, H. C., Chou, C. C. K., Lee, C. S. L., Kuo, W. C., and Chang, S. C.: Hygroscopic properties and cloud condensation nuclei activity of atmospheric aerosols under the influences of Asian continental outflow and new particle formation at a coastal site in eastern Asia, Atmos. Chem. Phys., 20, 5911-5922, 10.5194/acp-20-5911-2020, 2020.

Dumka, U. C., Bhattu, D., Tripathi, S. N., Kaskaoutis, D. G., and Madhavan, B. L.: Seasonal inhomogeneity in cloud precursors over Gangetic Himalayan region during GVAX campaign, Atmospheric Research, 155, 158-175, https://doi.org/10.1016/j.atmosres.2014.11.022, 2015.

Jayachandran, V. N., Suresh Babu, S. N., Vaishya, A., Gogoi, M. M., Nair, V. S., Satheesh, S. K., and Krishna Moorthy, K.: Altitude profiles of cloud condensation nuclei characteristics across the Indo-Gangetic Plain prior to the onset of the Indian summer monsoon, Atmos. Chem. Phys., 20, 561-576, 10.5194/acp-20-561-2020, 2020.

Jin, Q., Grandey, B. S., Rothenberg, D., Avramov, A., and Wang, C.: Impacts on cloud radiative effects induced by coexisting aerosols converted from international shipping and maritime DMS emissions, Atmos. Chem. Phys., 18, 16793-16808, 10.5194/acp-18-16793-2018, 2018.

Kettle, A. J., Andreae, M. O., Amouroux, D., Andreae, T. W., Bates, T. S., Berresheim, H., Bingemer, H., Boniforti, R., Curran, M. A. J., DiTullio, G. R., Helas, G., Jones, G. B., Keller, M. D., Kiene, R. P., Leck, C., Levasseur, M., Malin, G., Maspero, M., Matrai, P., McTaggart, A. R., Mihalopoulos, N., Nguyen, B. C., Novo, A., Putaud, J. P., Rapsomanikis, S., Roberts, G., Schebeske, G., Sharma, S., Simó, R., Staubes, R., Turner, S., and Uher, G.: A global database of sea surface dimethylsulfide (DMS) measurements and a procedure to predict sea surface DMS as a function of latitude, longitude, and month, Global Biogeochemical Cycles, 13, 399-444, 10.1029/1999GB900004, 1999.

Lana, A., Bell, T. G., Simó, R., Vallina, S. M., Ballabrera-Poy, J., Kettle, A. J., Dachs, J., Bopp, L., Saltzman, E. S., Stefels, J., Johnson, J. E., and Liss, P. S.: An updated climatology of surface dimethlysulfide concentrations and emission fluxes in the global ocean, Global Biogeochemical Cycles, 25, 10.1029/2010GB003850, 2011.

Leena, P. P., Pandithurai, G., Anilkumar, V., Murugavel, P., Sonbawne, S. M., and Dani, K. K.: Seasonal variability in aerosol, CCN and their relationship observed at a high altitude site in Western Ghats, Meteorology and Atmospheric Physics, 128, 143-153, 10.1007/s00703-015-0406-0, 2016.

Li, S., Sarwar, G., Zhao, J., Zhang, Y., Zhou, S., Chen, Y., Yang, G., and Saiz-Lopez, A.: Modeling the Impact of Marine DMS Emissions on Summertime Air Quality Over the Coastal East China Seas, Earth and Space Science, 7, e2020EA001220, https://doi.org/10.1029/2020EA001220, 2020a.

Li, S., Zhang, Y., Zhao, J., Sarwar, G., Zhou, S., Chen, Y., Yang, G., and Saiz-Lopez, A.: Regional and Urban-Scale Environmental Influences of Oceanic DMS Emissions over Coastal China Seas, Atmosphere, 11, 10.3390/atmos11080849, 2020b.

Liu, C., Wang, T., Rosenfeld, D., Zhu, Y., Yue, Z., Yu, X., Xie, X., Li, S., Zhuang, B., Cheng, T., and Niu, S.: Anthropogenic Effects on Cloud Condensation Nuclei Distribution and Rain Initiation in East Asia, Geophysical Research Letters, 47, e2019GL086184, https://doi.org/10.1029/2019GL086184, 2020.

Mahajan, A. S., Fadnavis, S., Thomas, M. A., Pozzoli, L., Gupta, S., Royer, S.-J., Saiz-Lopez, A., and Simó, R.: Quantifying the impacts of an updated global dimethyl sulfide climatology on cloud microphysics and aerosol radiative forcing, Journal of Geophysical Research: Atmospheres, 120, 2524-2536, https://doi.org/10.1002/2014JD022687, 2015.

Rap, A., Scott, C. E., Spracklen, D. V., Bellouin, N., Forster, P. M., Carslaw, K. S., Schmidt, A., and Mann, G.: Natural aerosol direct and indirect radiative effects, Geophysical Research Letters, 40, 3297-3301, https://doi.org/10.1002/grl.50441, 2013.

Roy, A., Chatterjee, A., Sarkar, C., Das, S. K., Ghosh, S. K., and Raha, S.: A study on aerosol-cloud condensation nuclei (CCN) activation over eastern Himalaya in India, Atmospheric Research, 189, 69-81, https://doi.org/10.1016/j.atmosres.2017.01.015, 2017.

Schmidtko, S., Johnson, G. C., and Lyman, J. M.: MIMOC: A global monthly isopycnal upper-ocean climatology with mixed layers, Journal of Geophysical Research: Oceans, 118, 1658-1672, https://doi.org/10.1002/jgrc.20122, 2013.

Thomas, M. A., Suntharalingam, P., Pozzoli, L., Rast, S., Devasthale, A., Kloster, S., Feichter, J., and Lenton, T. M.: Quantification of DMS aerosol-cloud-climate interactions using the ECHAM5-HAMMOZ model in a current climate scenario, Atmos. Chem. Phys., 10, 7425-7438, 10.5194/acp-10-7425-2010, 2010.

Varghese, M., Prabha, T. V., Malap, N., Resmi, E. A., Murugavel, P., Safai, P. D., Axisa, D., Pandithurai, G., and Dani, K.: Airborne and ground based CCN spectral characteristics: Inferences from CAIPEEX – 2011, Atmospheric Environment, 125, 324-336, https://doi.org/10.1016/j.atmosenv.2015.06.041, 2016.

Wang, W. L., Song, G., Primeau, F., Saltzman, E. S., Bell, T. G., and Moore, J. K.: Global ocean dimethyl sulfide climatology estimated from observations and an artificial neural network, Biogeosciences, 17, 5335-5354, 10.5194/bg-17-5335-2020, 2020.

Yang, G.-P., Song, Y.-Z., Zhang, H.-H., Li, C.-X., and Wu, G.-W.: Seasonal variation and biogeochemical cycling of dimethylsulfide (DMS) and dimethylsulfoniopropionate (DMSP) in the Yellow Sea and Bohai Sea, Journal of Geophysical Research: Oceans, 119, 8897-8915, https://doi.org/10.1002/2014JC010373, 2014.

Yang, G.-P., Zhang, S.-H., Zhang, H.-H., Yang, J., and Liu, C.-Y.: Distribution of biogenic sulfur in the Bohai Sea and northern Yellow Sea and its contribution to atmospheric sulfate aerosol in the late fall, Marine Chemistry, 169, 23-32, https://doi.org/10.1016/j.marchem.2014.12.008, 2015a.
Yang, J., Yang, G., Zhang, H., and Zhang, S.: Spatial distribution of dimethylsulfide and dimethylsulfoniopropionate in the Yellow Sea and Bohai Sea during summer, Chinese Journal of Oceanology and Limnology, 33, 1020-1038, 10.1007/s00343-015-4188-5, 2015b.
Yang, Y., Wang, H., Smith, S. J., Easter, R., Ma, P. L., Qian, Y., Yu, H., Li, C., and Rasch, P. J.: Global source attribution of sulfate concentration and direct and indirect radiative forcing, Atmos. Chem. Phys., 17, 8903-8922, 10.5194/acp-17-8903-2017, 2017.